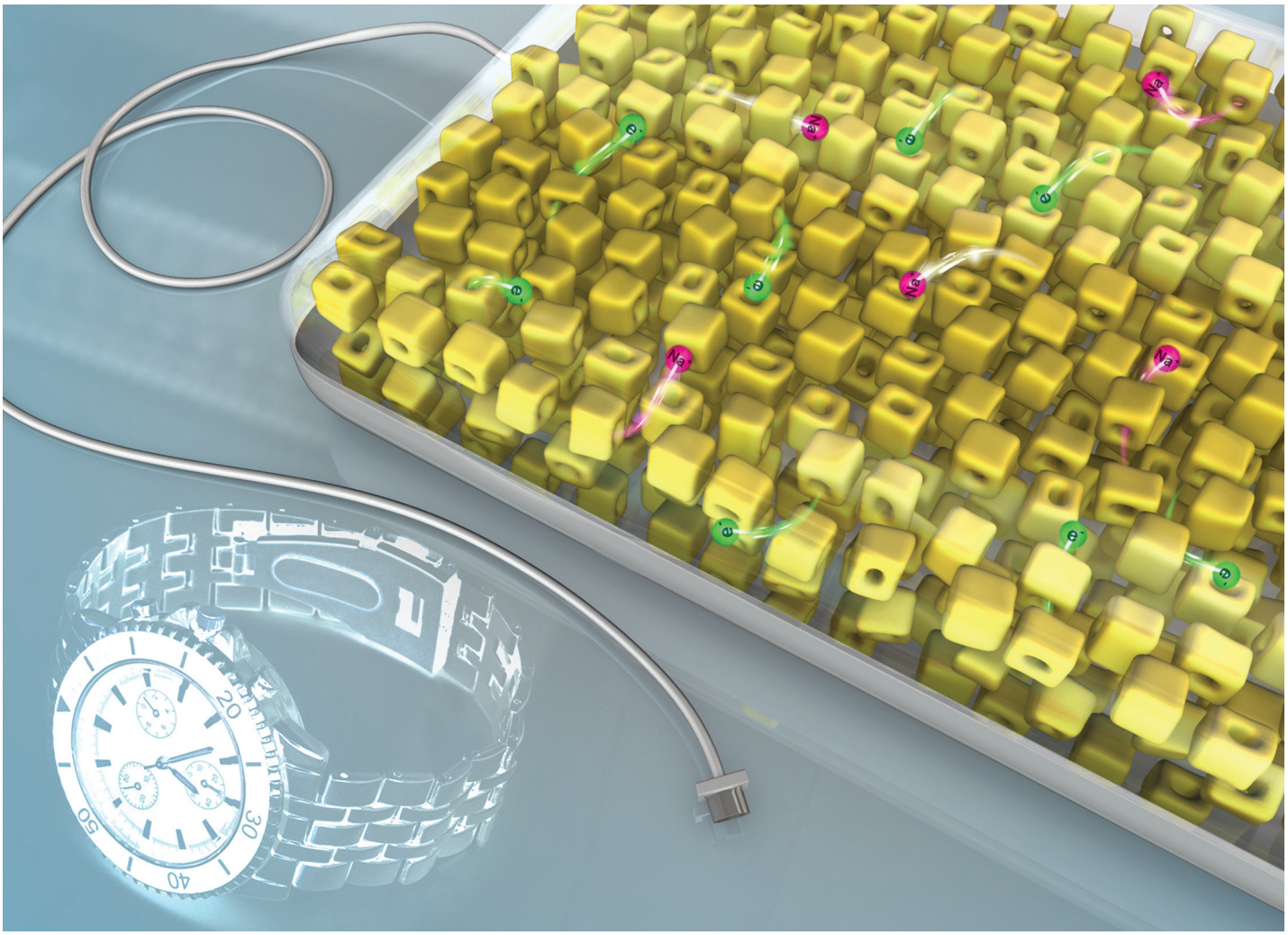

Showcasing research from the School of Advanced Materials, Peking University Shenzhen Graduate School, Shenzhen, China.

An open holey structure enhanced rate capability in a $NaTi_2(PO_4)_3$/C nanocomposite and provided ultralong-life sodium-ion storage

Sodium-ion battery (SIB) technology is competitive in the fields of transportation and grid storage, in which electrode materials with rapid energy conversion and long cycle life need to be identified. The work shows a newly synthesized $NaTi_2(PO_4)_3$/C nanocomposite with an open holey-structured framework. The nanocomposite realizes fast sodium-ion transport and thus preferable battery performances. Tailoring the open channels for ion transport was proven to contribute to such performance enhancement and therefore holds potential to become a universal model toward the development of sustainable electrode materials in SIBs and other battery systems.

As featured in:

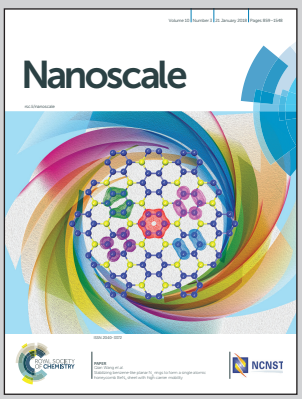

See Mianqi Xue, Rui Li *et al.*, *Nanoscale*, 2018, **10**, 958.

ROYAL SOCIETY OF CHEMISTRY

rsc.li/nanoscale

Registered charity number: 207890

Nanoscale

PAPER

View Article Online
View Journal | View Issue

Cite this: *Nanoscale*, 2018, **10**, 958

An open holey structure enhanced rate capability in a $NaTi_2(PO_4)_3$/C nanocomposite and provided ultralong-life sodium-ion storage†

Liuxin Zhang,[a] Xusheng Wang,[b] Wenjun Deng,[a] Xiaoling Zang,[c] Chunyi Liu,[a] Chang Li,[a] Jitao Chen,[b] Mianqi Xue, *[a,c] Rui Li*[a] and Feng Pan [a]

Received 19th September 2017,
Accepted 6th November 2017

DOI: 10.1039/c7nr07000d

rsc.li/nanoscale

Sodium-ion battery (SIB) technology is competitive in the fields of transportation and grid storage, which require electrode materials showing rapid energy conversion (high rate capability) and long cycle life. In this work, a $NaTi_2(PO_4)_3$/C (NTP/C) nanocomposite with an open holey-structured framework was successfully prepared for the first time using a solvothermal reaction followed by pyrolysis. The nanocomposite realized fast sodium-ion transport and thus preferable battery performances. Within the wide rate range of 0.5–50C, only a very small decrease in capacity from 124 to 120 mA h g^{-1} was observed. A high discharge capacity of 103 mA h g^{-1} (88.3% retention of the 1st cycle) was delivered even after 10 000 cycles at an ultrahigh rate of 50C without any obvious morphological change and without structural pulverization. Forming open channels for ion transport proved to contribute to such performance enhancement and therefore has the potential to become a universal model for the development of sustainable electrode materials in SIBs and other battery systems.

Introduction

In addition to lithium-ion batteries,[1] rechargeable sodium-ion batteries (SIBs) have demonstrated great potential as practical devices for transportation and grid storage along with other charge-storage devices (such as traditional capacitors, electrets, and supercapacitors) and other kinds of ion batteries.[2–4] The continuous demands for faster energy conversion, more stable and long-lived energy-storage and automotive devices, and more cost- and eco-friendly routes for achieving these features challenge us to design better electrode materials for SIBs to satisfy these needs.[5,6] In this regard, sodium superionic conductor (NASICON)-type compounds, which show high sodium-ion conductivity and small volume expansion, should provide a large platform from which to fabricate more sustainable electrodes.[7,8] $NaTi_2(PO_4)_3$ (NTP), whose framework consists of corner-shared PO_4 tetrahedra and TiO_6 octahedra with Na atoms situated in the tunnels, is an attractive example of a NASICON-type compound.[9–11]

Similar to the research carried out to enhance the performance of $LiFePO_4$, which otherwise shows low electronic conductivity,[12,13] the strategy of coupling carbon species with NTP composites has been shown to improve cycling stability.[8–11,14,15] Another practical difficulty is how to access an adequate amount of sodium ions to receive electrons at the reaction sites in a short amount of time. Hence, there is a need to improve the rate capability by improving electron transport and speeding up sodium-ion transport. Previous studies of NTP composites have made considerable progress in addressing these problems, yet achieving a combination of ultrafast sodium-ion storage, ultralong lifetime, and high capacity retention, all necessary for further practical applications, is still a challenge.[8–11,14–19]

Producing an open framework in carbon-coated nanostructured materials could improve electronic conductivity and facilitate ion transport, thus allowing for a high rate capability and full capacity delivery by implementing sufficient transport of charges (both the electrons and ions) in a given cycle duration.[20] Based on this strategy, an open holey-structured $NaTi_2(PO_4)_3$/C (NTP/C) nanocomposite was successfully prepared for the first time by setting the solvothermal treatment time to 24 h (resulting in a product denoted as NTP/C-24 h). The synthesis of NTP/C-24 h then also involved the same pyrolysis process as used for the NTP/C-6 h and NTP/C-48 h nano-

[a]*School of Advanced Materials, Peking University Shenzhen Graduate School, Shenzhen 518055, China. E-mail: lirui@pkusz.edu.cn*
[b]*Beijing National Laboratory for Molecular Sciences College of Chemistry and Molecular Engineering, Peking University, Beijing 100871, China*
[c]*Institute of Physics and Beijing National Laboratory for Condensed Matter Physics Chinese Academy of Sciences, Beijing 100190, China. E-mail: xuemq@iphy.ac.cn*
†Electronic supplementary information (ESI) available: Experimental section, TGA morphology characterization, other electrochemical performances. See DOI: 10.1039/c7nr07000d

composites. Faster sodium-ion transport and thus much enhanced electrochemical performances were realized in the NTP/C-24 h nanocomposite. Increasing the rate of the NTP/C-24 h nanocomposite from 0.5 to 50C caused only a negligible capacity loss from 124 to 120 mA h g^{-1} in the NTP/C-24 h nanocomposite, indicating efficient sodium-ion transport in this nanocomposite even at a short discharge (charge) time of 1.2 min (at a 50C rate). Furthermore, the NTP/C-24 h nanocomposite demonstrated a high capacity retention of 103 mA h g^{-1} (88.3% of the 1st cycle) even after 10 000 cycles at the ultrahigh 50C rate with no obvious damage in morphology and structure. The open holey-structured nanomaterial and nanocomposite systems should become a promising model for achieving the combination of ultrafast ion storage, ultralong life time, and high capacity retention for the development of sustainable electrode materials in SIBs and other battery systems.

Results and discussion

A schematic of the process used to synthesize the NTP/C nanocomposites is shown in Fig. 1. The NTP/C-6 h, NTP/C-24 h, and NTP/C-48 h nanocomposites were prepared using the same solvothermal procedure, except for the different reaction times of 6, 24, and 48 h. Comparison of the X-ray diffraction (XRD) patterns of the nanocomposites (Fig. 2a) indicated all of them to exhibit features typical of crystalline NTP except that the NTP/C-6 h was contaminated by the TiP_2O_7 crystalline phases, indicating the solvothermal time of 6 h to be inadequate for achieving the full growth of NTP species. Meanwhile, typical XRD peaks of crystalline graphite were not observed for any of the nanocomposites, suggesting the amorphous nature of the coated carbon, which did not affect the crystal structure of NTP. The results of thermogravimetric analyses (TGA) of the three NTP/C nanocomposites (Fig. S1, ESI†) revealed their carbon contents to all be nearly the same, at ~5 wt%.

The morphologies of the NTP/C-6 h, NTP/C-24 h, and NTP/C-48 h nanocomposites were assessed by performing scanning electron microscopy (SEM) (Fig. 2b–d). The SEM image of the NTP/C-6 h nanocomposite (Fig. 2b) showed nanoparticles that

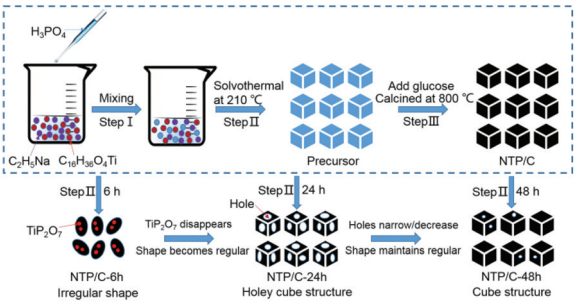

Fig. 1 Schematic illustration of the preparation of the NTP/C nanocomposites. The NTP/C-6, NTP/C-24 h, and NTP/C-48 h nanocomposites were synthesized by first carrying out solvothermal treatment for 6, 24, and 48 h, respectively, and then pyrolysis.

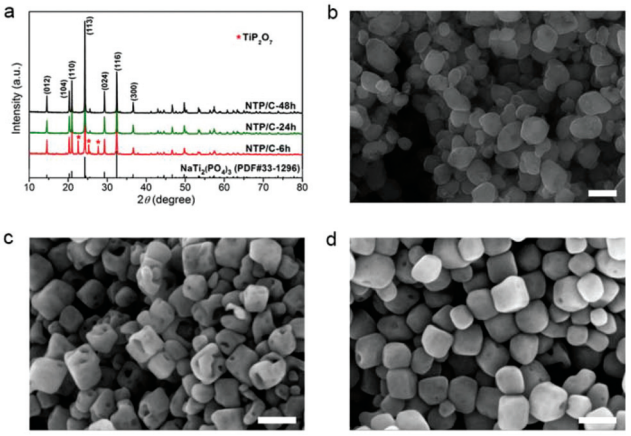

Fig. 2 (a) XRD patterns of the NTP/C nanocomposites. All of the nanocomposites exhibited typical features of crystalline NTP except that the NTP/C-6 h species was contaminated with the TiP_2O_7 crystalline phases. (b, c, d) SEM images of the NTP/C-6, NTP/C-24 h, and NTP/C-48 h nanocomposites, respectively. The NTP/C nanocomposites showed similar average particle sizes, and only the NTP/C-24 h nanocomposite showed the open holey-structured framework. The scale bars represent 200 nm in panels (b–d).

appeared irregular in both the shape and size (with an average size of less than 200 nm). The SEM image of NTP/C-24 h (Fig. 2c) showed the presence of particles with various sizes, but also displaying open holey-structured nanocube morphologies with an average hole size of less than 50 nm. The image of the NTP/C-48 h nanocomposite (Fig. 2d) showed more regular nanocubes, and without hardly any holes, with this near absence of holes was attributed to the extended solvothermal treatment time of 48 h. While the three NTP/C nanocomposites were similar with regards to average particle size, being less than 200 nm, they differed with regards to particle shape and open holey structure. A transmission electron microscopy (TEM) image of the NTP/C-6 h nanocomposite (Fig. S2a, ESI†), however, revealed the presence of holes. This observation for the NTP/C-6 h nanocomposite, together with its morphology as shown in its SEM image (Fig. 2b), indicated the holes to be located in the interior of the particles, without channels extending to the particle surface. Analysis of the high-resolution TEM (HRTEM) image of the NTP/C-6 h nanocomposite (Fig. S2b, ESI†) further confirmed the interior locations of the holes. And the marked *d*-spacing of 0.43 nm of the selected area electron diffraction (SAED) pattern (the inset) was assigned to the (110) crystal plane of hexagonal NTP. The TEM image of the NTP/C-24 h nanocomposite (Fig. 3a) demonstrated the open holey structures spanning the nanocubes, consistent with the morphology indicated by its SEM image in Fig. 2c. The (012) crystal plane in the hexagonal NTP was identified in its HRTEM image (see that of the NTP/C-24 h nanocomposite in Fig. 3b) by the marked *d*-spacing of 0.61 nm and the SAED pattern (the inset). As for the NTP/C-48 h nanocomposite, its TEM image (Fig. S2c (ESI†)) showed interior holes similar to those of the NTP/C-6 h nanocomposite. And

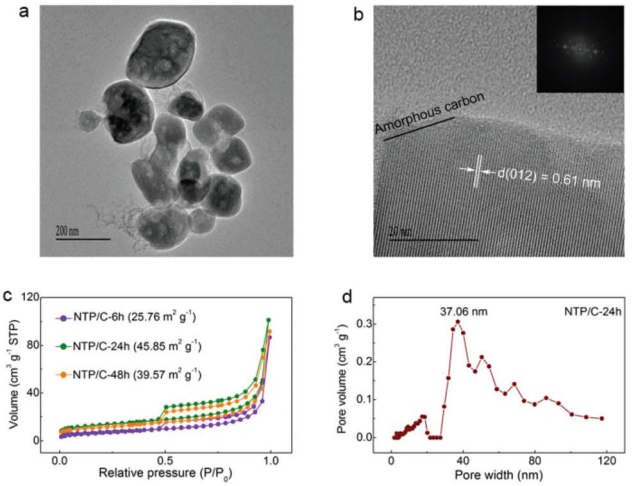

Fig. 3 (a) TEM image of the NTP/C-24 h nanocomposite, with the image showing particles containing holes extending throughout the particle. (b) HRTEM image of the NTP/C-24 h nanocomposite. A layer of carbon coating the particle was observed and the marked *d*-spacing of 0.61 nm was assigned to the (012) crystal plane. The inset shows the corresponding SAED pattern. (c) Nitrogen adsorption/desorption isotherms of the NTP/C-6 h, NTP/C-24 h, and NTP/C-48 h nanocomposites. The NTP/C-24 h nanocomposite showed the largest specific surface area. (d) Pore size distribution of the NTP/C-24 h nanocomposite, showing an average pore size of 37.06 nm, in the mesopore range.

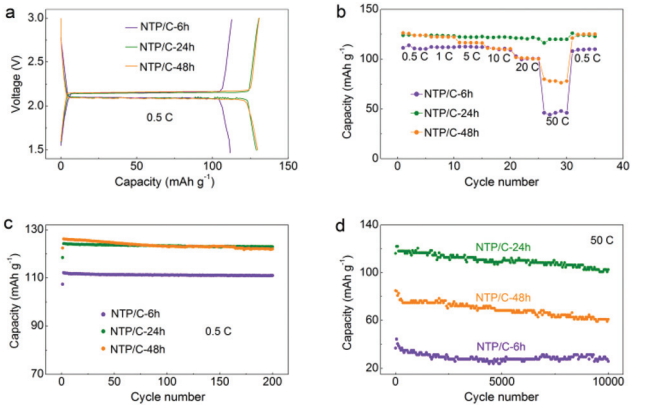

Fig. 4 Electrochemical performances of the NTP/C electrodes. (a) Galvanostatic voltage profiles of the NTP/C electrodes cycled at a rate of 0.5C. A flat discharge plateau at about 2.1 V and a very small voltage hysteresis were observed. (b) Rate capability of the NTP/C electrodes. The NTP/C-24 h electrode performed best, with a high discharge capacity of 120 mA h g^{-1} at the ultrahigh rate of 50C. (c) Cycling performances of the NTP/C electrodes. A high discharge capacity of 123 mA h g^{-1} was delivered after 200 cycles at a 0.5C rate without capacity fading for the NTP/C-24 h electrodes. (d) Long-term cycling performances of the NTP/C electrodes (1st, 50th, 100th, 150th, 200th, ..., 9900th, 9950th, and 10000th cycles are listed). The NTP/C-24 h electrodes revealed a high discharge capacity of 103 mA h g^{-1} (88.3% of the 1st cycle) even after 10 000 cycles at the ultrahigh 50C rate.

its HRTEM image (Fig. S2d, ESI†) also showed the (012) crystal plane. The above results taken together indicated the presence of holes in the interiors of all of the NTP/C nanocomposite particles but of holes spanning the particles from the interior to the surface only for NTP/C-24 h. The results also revealed the presence of uniform carbon layers with an average thickness of less than 5 nm coating the particles of all of the NTP/C nanocomposites, with such carbon coatings improving the electronic conductivity.

To further evaluate the holey structure of the NTP/C nanocomposites, a BET analysis was carried out. The specific surface areas of the NTP/C-6 h, NTP/C-24 h, and NTP/C-48 h nanocomposites were measured, based on their nitrogen adsorption/desorption isotherms (Fig. 3c), to be 25.76, 45.85, and 39.57 $m^2\ g^{-1}$, in accordance with the morphological and microstructural analyses indicating holes extending from the particle interior to the particle surface only for the NTP/C-24 h nanocubes. Fig. 3d shows the pore size distribution of the NTP/C-24 h nanocomposite; the average width of the pores was determined to be 37.06 nm, based on the Barrett–Joyner–Halenda model ($t = 3.54[-5\ln(P/P_0)]^{0.333}$). Thus, by appropriately setting the duration of the solvothermal treatment, to 24 h, we were able to fabricate NTP/C nanocubes displaying holes extending throughout the cube, and hence having high specific surface areas and mesopore features; these features were expected to facilitate sodium-ion transport and improve the wettability of the electrolyte and hence yield a better rate capability and cycling stability.

The electrochemical performances of the NTP/C nanocomposites were measured and compared in order to assess the effect of the extensive holes. As shown in Fig. 4a, the galvanostatic voltage profiles of the NTP/C electrodes cycled at 0.5C (1C corresponds to 133 mA g^{-1}, 1.5–3.0 V) showed a flat discharge plateau at about 2.1 V (corresponding to the sodium-ion intercalation process) and a very small voltage hysteresis, which could ensure a high level of energy efficiency. All three NTP/C species showed hardly any irreversibility in the first sodiation/desodiation process. And high discharge capacities of 112, 129, and 130 mA h g^{-1} were separately delivered for the NTP/C-6 h, NTP/C-24 h, and NTP/C-48 h electrodes (the delivered capacities of the three NTP/C nanocomposites were all calculated based on the mass of the whole NTP/C). Rate capability tests of the NTP/C electrodes were carried out by applying rates of 0.5, 1, 5, 10, 20, and 50C each for five cycles at a time (Fig. 4b). The NTP/C-24 h electrode displayed a discharge capacity of 120 mA h g^{-1}, at a rate of 50C, much higher than the values of 46 and 78 mA h g^{-1} for the NTP/C-6 h and NTP/C-48 h electrodes, respectively. Furthermore, a negligible capacity loss from 124 to 120 mA h g^{-1} (from 0.5 to 50C) occurred for the NTP/C-24 h electrodes, indicating a strong promotion of sodium-ion transport by the extensive holes in these nanocomposite particles. The cycling performances of the NTP/C electrodes were also investigated. As shown in Fig. 4c, the NTP/C-6 h, NTP/C-24 h, and NTP/C-48 h electrodes showed discharge capacities of 111, 123, and 122 mA h g^{-1} after 200 cycles at 0.5C, and no significant decrease in capacity with increasing cycle number occurred for the NTP/C-24 h

electrodes. The capacity retention was expected to be more differentiated for the NTP/C electrodes at the higher rate. As shown in Fig. 4d, a high discharge capacity of 103 mA h g^{-1} (88.3% of the 1st cycle) was measured for the NTP/C-24 h electrodes even after 10 000 cycles at the ultrahigh rate of 50C. The corresponding values were only 26 mA h g^{-1} (70.0% of the 1st cycle) and 61 mA h g^{-1} (71.7% of the 1st cycle) for the NTP/C-6 h and NTP/C-48 h electrodes, respectively. The open holey-structured framework in the NTP/C-24 h nanocomposite significantly facilitated the sodium-ion transport and improved the structural maintenance, thus yielding a much higher retention of capacity and cycling stability than shown by the NTP/C-6 h and NTP/C-48 h nanocomposites. As displayed in Fig. 5, the electrochemical performances of the NTP/C-24 h electrodes ranked toward the top among the group of some of the best-performing published NTP materials with regards to rate, cycle life, and capacity retention (only works of over 1000 cycles were selected for this comparison).[9–11,14–19,21–26]

To further study the relationship between the open holey-structured framework and electrochemical performances, cyclic voltammetry (CV) curves scanned at various rates, specifically of 0.1, 0.2, and 0.5 mV s^{-1} (1.5–3.0 V), were acquired for the NTP/C-6 h, NTP/C-24 h, and NTP/C-48 h electrodes, as shown in Fig. S3a–3c (ESI†). A pair of well-defined peaks was observed in each of the CV curves, consistent with the galvanostatic voltage profiles, shown in Fig. 4a. The diffusion coefficient of sodium ions in the NTP/C nanocomposites were estimated using the equation $I_P = 2.69 \times 10^{-5} An^{3/2} C_0 D^{1/2} v^{1/2}$, in which I_p is the peak current, A is the electrode contact area (A is 0.78 cm^2 in this work), n is the number of electrons during the sodiation process of per NTP molecule (n is 2 in this work), C_0 is the concentration of sodium ions (C_0 is 1 mol L^{-1} in this work), D is the diffusion efficient of sodium ions, and v is the scan rate. Therefore, by producing a linear fit of the peak current as a function of the square root of the scan rate (Fig. S3d, ESI†), the sodium-ion diffusion coefficients for the NTP/C-6 h, NTP/C-24 h, and NTP/C-48 h nanocomposites were determined to be 1.91×10^{-10}, 1.51×10^{-9}, and 7.45×10^{-10} cm^2 s^{-1}, respectively, in good agreement with the above analyses, and indicating the strong benefits of the open holey-structured framework in the NTP/C-24 h nanocomposites.

A further assessment of the kinetics of the NTP/C electrodes was conducted by acquiring and comparing their electrochemical impedance spectroscopy (EIS) patterns after 5 and 10 000 cycles. The top inset of Fig. 6a shows a schematic of the equivalent circuit; in this figure, R_b, C_{dl}, R_{ct}, and Z_w represent the bulk resistance, constant phase element, charge-transfer resistance, and Warburg impedance. The R_{ct} values of the NTP/C-6 h, NTP/C-24 h, and NTP/C-48 h electrodes each after 5 cycles were determined to be 184.3, 101.7, and 148.8 Ω, while those after 10 000 cycles were determined to be 410.6, 197.9, and 268.9 Ω, respectively (Fig. 6b). The NTP/C-24 h electrode exhibited the lowest charge-transfer resistance among all the samples at the 50C rate, both after 5 cycles and after 10 000 cycles. The charge-transfer resistance values after 10 000 cycles were larger than those after just 5 cycles for all the three NTP/C species. At the ultrahigh rate of 50C, an interfacial reaction between the NTP/C surface and liquid electrolyte would have been expected to occur during the long-term cycling process. The generated resistive layer may have hindered sodium-ion transport at the NTP/C active particle/liquid electrolyte interface, which would consequently deteriorate the cycling stability.[27] Yet, of all the nanocomposites, NTP/C-24 h demon-

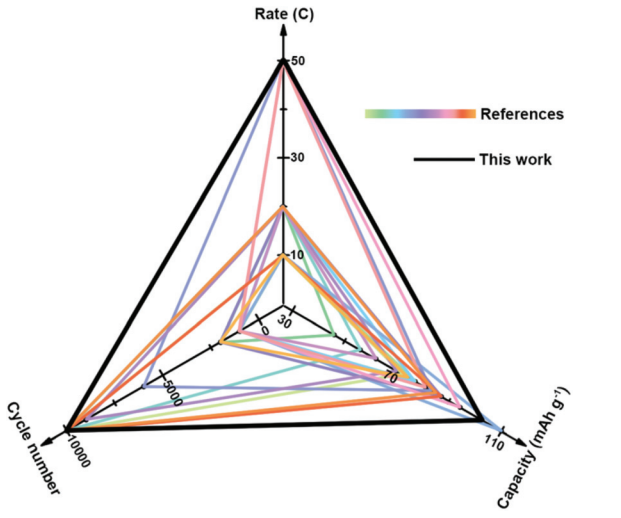

Fig. 5 The long-lived cycling performances of the NTP/C-24 h electrodes compared to those of some of the previous reported NTP materials. (Only works of over 1000 cycles were selected.) The rate, cycle life, and capacity retention of the NTP/C-24 h electrodes all ranked near the top among those for various the NTP materials.[9–11,14–19,21–26]

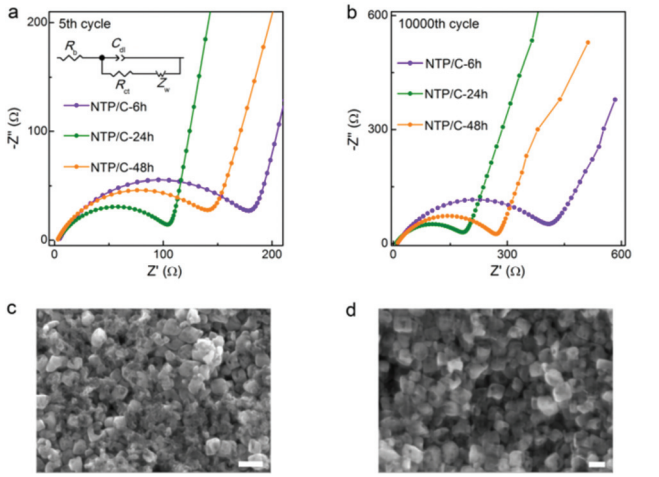

Fig. 6 (a, b) EIS patterns of the NTP/C electrodes at a 50C rate after (a) 5 and (b) 10 000 cycles. The NTP/C-24 h electrode exhibited the smallest charge-transfer resistance after both the 5th and 10000th cycles. The top inset in panel (a) shows a diagram of the equivalent circuit. (c) SEM image of the initial NTP/C-24 h electrode, and (d) that after 10 000 cycles at a 50C rate. The nanocubes remained intact without any considerbale change in morphology and without their structures being pulverized even after the 10 000 cycles. The scale bars represent 300 and 200 nm in panels (c) and (d), respectively.

strated the smallest increase of charge-transfer resistance from the 5th to 10000th cycle, indicating its high cycling stability. The morphologies of the NTP/C-24 h electrode before being used and after 10 000 cycles (at 50C rate) were compared to provide a structural explanation for its superior cycling stability. As shown in Fig. 6c, the NTP/C-24 h electrode initially displayed a combination of nanocubes and conductive particles. The NTP/C-24 h electrode nanocubes remained intact, without any considerable change in their morphology and certainly without having their structures pulverized, even after 10 000 cycles (Fig. 6d). These results taken together indicated that the open holey-structured framework can endow the electrode with strong structural stability in the face of long-duration ultrafast sodium-ion transport, and that superior battery performances are accessible to the NTP/C-24 h nanocomposite.

Conclusions

In summary, an open holey-structured NTP/C nanocomposite was synthesized for the first time by setting the solvothermal treatment time to 24 h. The synthesis of this NTP/C-24 h nanocomposite then used the same pyrolysis treatment as was used for the NTP/C-6 h and NTP/C-48 h nanocomposites. The NTP/C-24 h nanocomposite showed a behavior indicative of faster sodium-ion transport and thus much improved battery performances. A negligible decrease in capacity from 124 to 120 mA h g^{-1} in the NTP/C-24 h nanocomposite occurred even as the rate was increased from 0.5 to 50C, indicating a very efficient sodium-ion transport at a very short discharge (charge) duration of 1.2 min (at a rate of 50C). Moreover, a high capacity retention of 103 mA h g^{-1} (88.3% of the 1st cycle) was achieved even after 10 000 cycles at a rate of 50C for the NTP/C-24 h nanocomposite. The open holey framework significantly facilitated the sodium-ion transport, thus allowing the ultrafast and long-lived discharge/charge processes without any obvious change in morphology and pulverization in structure. Such systems consisting of open holey-structured nanomaterials and nanocomposites (and including a conducting polymer,[28] graphene[29] or other metal chalcogenides[30] for enhancing conductivity and capacity) should offer a promising model for achieving the combination of ultrafast ion storage, ultralong life time, and high capacity retention for the development of sustainable electrode materials in SIBs and other battery systems.

Conflicts of interest

There are no conflicts to declare.

Acknowledgements

This work was supported by the Shenzhen Science and Technology Research Grant (JCYJ20160531141109132, JCYJ20170412150450297), the National Natural Science Foundation of China (21622407) and Guangdong Innovative and Entrepreneurial Research Team Progress (2013N080).

Notes and references

1 C. Grey and J. Tarascon, *Nat. Mater.*, 2017, **16**, 45–56.
2 N. Yabuuchi, K. Kubota, M. Dahbi and S. Komaba, *Chem. Rev.*, 2014, **114**, 11636–11682; M. D. Slater, D. Kim, E. Lee and C. S. Johnson, *Adv. Funct. Mater.*, 2013, **23**, 947–958; Z. Hu, L. Wang, K. Zhang, J. Wang, F. Cheng, Z. Tao and J. Chen, *Angew. Chem., Int. Ed.*, 2014, **53**, 12794–12798; H. Pan, Y.-S. Hu and L. Chen, *Energy Environ. Sci.*, 2013, **6**, 2338–2360.
3 M. Xue, D. Chen, X. Wang, J. Chen and G. Chen, *J. Mater. Chem. A*, 2015, **3**, 7715–7718; X. Ma, M. Xue, F. Li, J. Chen, D. Chen, X. Wang, F. Pan and G. Chen, *Nanoscale*, 2015, **7**, 8715–8719; X. Ma, D. Zhao, M. Xue, H. Wang and T. Cao, *Angew. Chem., Int. Ed.*, 2010, **49**, 5537–5540.
4 T. Koketsu, J. Ma, B. J. Morgan, M. Body, C. Legein, W. Dachraoui, M. Giannini, A. Demortière, M. Salanne and F. Dardoize, *Nat. Mater.*, 2017, **16**, 1142–1148.
5 X. Wang, D. Chen, Z. Yang, X. Zhang, C. Wang, J. Chen, X. Zhang and M. Xue, *Adv. Mater.*, 2016, **28**, 8645–8650; C. Wang, L. Wang, F. Li, F. Cheng and J. Chen, *Adv. Mater.*, 2017, **29**, 1702212.
6 H. Geng, J. Yang, Z. Dai, Y. Zhang, Y. Zheng, H. Yu, H. Wang, Z. Luo, Y. Guo, Y. Zhang, H. Fan, X. Wu, J. Zheng, Y. Yang, Q. Yan and H. Gu, *Small*, 2017, **13**, 1603490; H. Yu, J. Yang, H. Geng and C. Li, *Nanotechnology*, 2017, **28**, 145403.
7 S. Chen, C. Wu, L. Shen, C. Zhu, Y. Huang, K. Xi, J. Maier and Y. Yu, *Adv. Mater.*, 2017, 1700431.
8 Y. Zhao, Z. Wei, Q. Pang, Y. Wei, Y. Cai, Q. Fu, F. Du, A. Sarapulova, H. Ehrenberg, B. Liu and G. Chen, *ACS Appl. Mater. Interfaces*, 2017, **9**, 4709–4718.
9 Y. Fang, L. Xiao, J. Qian, Y. Cao, X. Ai, Y. Huang and H. Yang, *Adv. Energy Mater.*, 2016, **6**, 1502197.
10 Y. Jiang, J. Shi, M. Wang, L. Zeng, L. Gu and Y. Yu, *ACS Appl. Mater. Interfaces*, 2016, **8**, 689–695.
11 C. Wu, P. Kopold, Y.-L. Ding, P. A. van Aken, J. Maier and Y. Yu, *ACS Nano*, 2015, **9**, 6610–6618.
12 Z. H. Chen and J. R. Dahn, *J. Electrochem. Soc.*, 2002, **149**, A1184–A1189.
13 Y. Wang, Y. Wang, E. Hosono, K. Wang and H. Zhou, *Angew. Chem., Int. Ed.*, 2008, **47**, 7461–7465.
14 D. Wang, Q. Liu, C. Chen, M. Li, X. Meng, X. Bei, Y. Wei, Y. Huang, F. Du, C. Wang and G. Chen, *ACS Appl. Mater. Interfaces*, 2016, **8**, 2238–2246.
15 C. Xu, Y. Xu, C. Tang, Q. Wei, J. Meng, L. Huang, L. Zhou, G. Zhang, L. He and L. Mai, *Nano Energy*, 2016, **28**, 224–231.
16 J. Song, S. Park, J. Gim, V. Mathew, S. Kim, J. Jo, S. Kim and J. Kim, *J. Mater. Chem. A*, 2016, **4**, 7815–7822.
17 X. C. Dong, H. Geng, J. Yang, H. Yu and C. Li, *Mater. Chem. Front.*, 2017, **1**, 1435–1440.

18 G. Yang, H. Song, M. Wu and C. Wang, *J. Mater. Chem. A*, 2015, **3**, 18718–18726.
19 Y. Jiang, L. Zeng, J. Wang, W. Li, F. Pan and Y. Yu, *Nanoscale*, 2015, **7**, 14723–14729.
20 H. Sun, L. Mei, J. Liang, Z. Zhao, C. Lee, H. Fei, M. Ding, J. Lau, M. Li, C. Wang, X. Xu, G. Hao, B. Papandrea, I. Shakir, B. Dunn, Y. Huang and X. Duan, *Science*, 2017, **356**, 599–604; D. Chen, X. Wang, J. Chen, Z. Ren, M. Xue and G. Chen, *Adv. Mater.*, 2015, **27**, 4224–4228.
21 J. Yang, H. Wang, P. Hu, J. Qi, L. Guo and L. Wang, *Small*, 2015, **11**, 3744–3749.
22 X. Li, X. Zhu, J. Liang, Z. Hou, Y. Wang, N. Lin, Y. Zhu and Y. Qian, *J. Electrochem. Soc.*, 2014, **161**, A1181–A1187.
23 H.-K. Roh, H.-K. Kim, M.-S. Kim, D.-H. Kim, K. Y. Chung, K. C. Roh and K.-B. Kim, *Nano Res.*, 2016, **9**, 1844–1855.
24 B. Zhao, B. Lin, S. Zhang and C. Deng, *Nanoscale*, 2015, **7**, 18552–18560.
25 L. Wang, B. Wang, G. Liu, T. Liu, T. Gao and D. Wang, *RSC Adv.*, 2016, **6**, 70277–70283.
26 G. B. Xu, L. W. Yang, X. L. Wei, J. W. Ding, J. X. Zhong and P. K. Chu, *J. Power Sources*, 2016, **327**, 580–590.
27 J.-H. Park, J.-S. Kim, E.-G. Shim, K.-W. Park, Y. T. Hong, Y.-S. Lee and S.-Y. Lee, *Electrochem. Commun.*, 2010, **12**, 1099–1102; Y.-K. Sun, J.-M. Han, S.-T. Myung, S.-W. Lee and K. Amine, *Electrochem. Commun.*, 2006, **8**, 821–826.
28 M. Xue, F. Li, D. Chen, Z. Yang, X. Wang and J. Ji, *Adv. Mater.*, 2016, **28**, 8265–8270; M. Xue, Y. Wang, X. Wang, X. Huang and J. Ji, *Adv. Mater.*, 2015, **27**, 5923–5929; M. Xue, F. Li, Y. Wang, X. Cai, F. Pan and J. Chen, *Nanoscale*, 2013, **5**, 1803–1805; M. Q. Xue, X. L. Ma, Z. Xie, L. T. Duan, Y. Q. Jiang, M. N. Zhang and T. B. Cao, *Chem. – Asian J.*, 2010, **5**, 2266–2270.
29 Y. Liu, H. Liang, Z. Xu, J. Xi, G. Chen, W. Gao, M. Xue and C. Gao, *ACS Nano*, 2017, **11**, 4301–4306; H. Liang, X. Ma, Z. Yang, P. Wang, X. Zhang, Z. Ren, M. Xue and G. Chen, *Carbon*, 2016, **99**, 585–590.
30 Z. Yang, H. Liang, X. Wang, X. Ma, T. Zhang, Y. Yang, L. Xie, D. Chen, Y. Long, J. Chen, Y. Chang, C. Yang, X. Zhang, X. Zhang, B. Ge, Z. Ren, M. Xue and G. Chen, *ACS Nano*, 2016, **10**, 755–762; C. Wu, Y. Jiang, P. Kopold, P. A. van Aken, J. Maier and Y. Yu, *Adv. Mater.*, 2016, **28**, 7276–7283.